JOURNAL OF MATERIALS SCIENCE 19 (1984) 2561–2569

Effect of sliding friction forces on the strength of brittle materials

B. R. LAWN, S. M. WIEDERHORN, D. E. ROBERTS
Center for Materials Science, National Bureau of Standards, Washington, DC 20234, USA

A model is developed for the strength degradation of brittle surfaces in sliding contact with spherical indenters. The loss of strength is associated with the propagation of partial cone cracks in the wake of the indenter. Detailed fracture mechanics calculations are circumvented by working in the limit of ideal point-load contacts, with the key proposition that the crack dimensions remain insensitive to rotations of the cone axis relative to the specimen free surface. In this way the simple Roesler solution for classical, well-developed cone cracks may be retained as a convenient "reference state" for a more general theoretical description, whereby the superposition of a tangential friction force onto the normal loading is accommodated via a straightforward coordinate transformation operation. The major predictions of the model are tested by measuring the strengths of glass surfaces after contact with a sliding steel sphere. In particular, the degraded strengths are not strongly influenced by the coefficient of friction, contrary to expectations from some earlier indentation analyses.

1. Introduction

Brittle materials such as glasses and ceramics are highly susceptible to mechanical degradation by small-scale contact events. The degradation can include a microcracking component, and thereby result in severe losses in strength. Consequently, design criteria for brittle materials should strictly include some provision for assessing the contact loading history in prospective service environments. Considerable attention has been given to this problem under conditions of normal contact [1–5]; strength degradation formulae for surfaces subjected to either static or impact loading, with either "blunt" (elastic) or "sharp" (elastic–plastic) contacts, have been developed from indentation theory and tested extensively on glass specimens. The primary strength-controlling variables are the normal load pertinent to the dominant contact-induced flaw and the material toughness.

One contact configuration which has received relatively little attention in the context of strength degradation is that of sliding contact, in which a superposed "tangential" load augments the driving force for local fracture. Sliding contact is a potential problem in any ceramic system involving moving parts. It is, for instance, believed to be a major cause of failures in heat engines with ceramic stator and rotor components [6–8]. The best studied case of sliding contact is that of a sphere translating across a flat surface under conditions of constant friction and purely elastic deformation. Closed-form solutions for the stress fields [9], and numerical computations of crack evolution within these fields [10], are available for this case. The level of frictional stress at the contact interface is a critical factor in determining the intensity of the tensile component of the near field, and hence the normal load to initiate cracks from surface flaws. Essentially, the cracks assume the geometry of somewhat distorted Hertzian cones, i.e. "partial cones" [11], with their origins at the trailing edges of the contact circles. Several experimental studies have confirmed the main predictions of the earlier analyses, in qualitative if not quantitative detail [12–16]. Variants on the original calculations, e.g. taking "stick-slip" contact effects into account [17], merely reinforce the prevailing conviction that friction forces are highly deleterious to structural integrity.

0022–2461/84 $03.00 + .12

However, none of the above sliding damage studies explicitly addresses the question of strength degradation. Given that sliding does enhance crack initiation, what is the magnitude of the ensuing strength reduction once such cracks have propagated and arrested? It could be argued in the interest of conservative design that the initiation of contact fracture in brittle components is almost inevitable at some stage of service, in which case it is only the final crack configuration which requires specific consideration. This kind of argument is, of course, consistent with the "worst-case" design philosophy generally adopted by the glass and ceramic community. There is some attraction in having to deal with only the fully developed sliding-induced cracks, in that the near-contact complexities (e.g. stress-field inhomogeneities, surface flaw distributions) no longer exert a strong influence on the fracture mechanics. We shall accordingly apply this approach to the issue of strength degradation, with the ultimate aim of deriving an appropriately simple design equation in terms of the contact loading variables and material parameters.

In pursuit of this aim we retain the sphere-on-flat as our ideal sliding configuration, but circumvent the mathematical tedium of a full-scale fracture mechanics analysis [10, 18] by means of a stratagem. We adopt the well-known far-field solution for Hertzian cone cracks in normal loading [19] as our "reference state", and introduce a geometrical transformation scheme to incorporate frictional terms into this solution. Finally, we test the predictions of the resulting formulation on glass specimens subjected to a wide range of frictional sliding contact conditions.

2. Model for strength degradation in sliding contact

Our aim in this section is to construct a theoretical base for predicting strength characteristics of bodies subjected to frictional contacts. We take a free-sliding sphere as our model contact system, so that we may adopt the well-studied Hertzian cone crack as a convenient reference state for the fracture geometry. A complete analysis of the problem would require a detailed consideration of crack evolution through the elastic contact fields, embodying all the complications associated with uncertain flaw distributions (which determine the crack starting points) and with severe stress gradients (which determine the subsequent crack trajectories and energy release rates) [18]. We shall try to bypass these complications by focusing on far-field limiting solutions in which the incorporation of frictional tractions is achieved via a simple coordinate transformation scheme. This will provide us with a formulation for the effective crack size in terms of the contact variables, from which the degraded strength may be predicted.

2.1. Partial cone crack configurations

Let us begin with the classical cone crack configuration of Fig. 1 [11]. In the far-field approximation the normal load, P, is assumed to be concentrated at the cone tip. The cone geometry is specified by the dimension, c, and inclination angle, α. The solution for this case, first given by Roesler [19], has the simple form

$$c = (\eta P/K_c)^{2/3} \tag{1}$$

characteristic of all penny-like cracks (i.e. cracks with circular fronts) [20]; here η is a dimensionless quantity dependent on the cone angle α (in turn dependent on Poisson's ratio [18]) and K_c is the critical stress intensity factor for crack extension (toughness). Of course, implicit in the writing of this equation is the assumption that the load is sufficient to have initiated the cone crack in the first place.

How might Equation 1 for ideal axial loading be modified to allow for a superposed tangential sliding force? A useful clue is obtained from an earlier study of the surface topography around cone cracks in diamond [21]. It had long been known that the material outside the surface rim of the (truncated) cone suffers an appreciable uplift, but within this rim is barely displaced

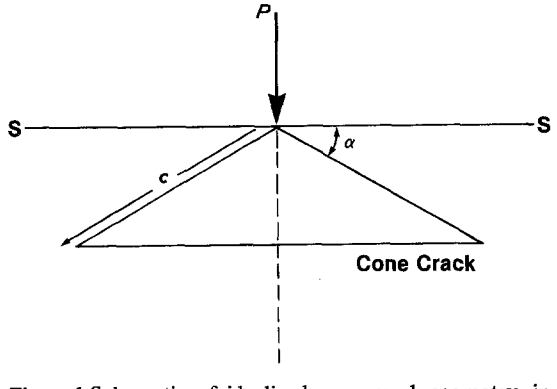

Figure 1 Schematic of idealized cone crack geometry, in far-field approximation. Normal force, P, is assumed to be concentrated at point on surface SS. Cone has characteristic dimension, c, inclination angle, α.

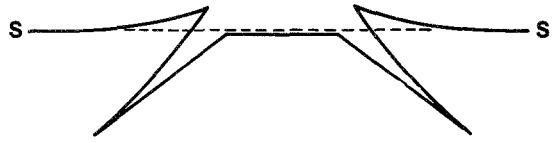

Figure 2 Schematic showing displacement configuration of cone crack walls at incompletely closed interface.

below its original level, Fig. 2. It was argued in this earlier study that the cone crack was being held open at its interface by fracture "debris". Since the cone walls tend to make shallow angles with the outer free surface, i.e. $\alpha \ll 90^\circ$, the "wedge shaped" portion of material in this region is relatively compliant, explaining the uplift. Within the surface rim the material is relatively rigid. The implication here is that the bulk of the applied loading prior to formation of the crack must be supported by the cone frustrum directly below the contact; that is, the displacement response of material outside the frustrum should be of little consequence to the energetics of the loading system. Indeed, in actual testing it is usually impossible to detect any load discontinuity on Hertzian crack pop-in unless elaborate sensing devices are used.

This conclusion leads us to the following ploy for accommodating the frictional component within the framework of the Roesler cone crack solution. We note first that, in the spirit of the point contact approximation, vectorial superposition of an appropriate tangential force, fP, increases the magnitude of the loading, to P' say, and rotates the line of action, through β say;

$$P' = P(1+f^2)^{1/2} \tag{2a}$$

$$\beta = \arctan f \tag{2b}$$

Hence the coefficient, f, is the sole determinant of our transformed load system. Now we make the key assertion that the essential geometry of the cone crack will remain unchanged by this transformation, except that the normal load is replaced by P' and the cone axis is rotated through β, to remain symmetrical about the line of action, as in Fig. 3. The rotational operation proposed here may be viewed equivalently as a simple tilt of the specimen surface relative to the contact axis in Fig. 1; and since material displacements outside the cone frustrum are of only secondary importance in their influence on the fracture mechanics, we may retain Equation 1 as the basis

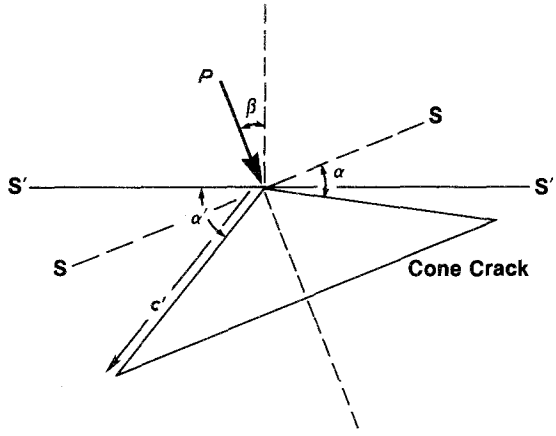

Figure 3 Hypothesized cone crack geometry for sliding contact case. Frictional force component is accommodated into scheme of Fig. 1 by an effective rotation of coordinates, equivalent to tilting the original surface SS through S'S'. Sliding direction left to right.

for determining the crack dimension appropriate to sliding contact. Accordingly, in conjunction with Equation 2, we obtain the slightly modified Roesler solution

$$c' = (\eta P'/K_c)^{2/3} = (\eta P/K_c)^{2/3}(1+f^2)^{1/3} \tag{3a}$$

The rotated cone on its steepest side then makes an angle

$$\alpha' = \alpha + \beta = \alpha + \arctan f \tag{3b}$$

with the specimen surface.

It is interesting to check the simplistic geometrical operation outlined above against more detailed, earlier determinations of partial-cone trajectories using computer codes [10]. Comparative predictions for two friction coefficients are shown in Fig. 4, taking $\alpha = 22^\circ$ for glass [19]. It is seen that the present model captures the essence of the computer evaluations, allowing that the latter includes provision for a non-zero area of contact. We may also note that the cone base actually intersects the specimen free surface in Fig. 4b; we see from Fig. 3 that the condition for this type of intersection is that $\beta > \alpha$, or, from Equation 2b, that $f > \tan\alpha = 0.4$ for glass. Again, the diagrams depict a single crack in each case, whereas most sliding contacts generate a series of such cracks (usually with reasonably regular spacing). We shall ignore any such perturbations on the ideal cone geometry, on the grounds that

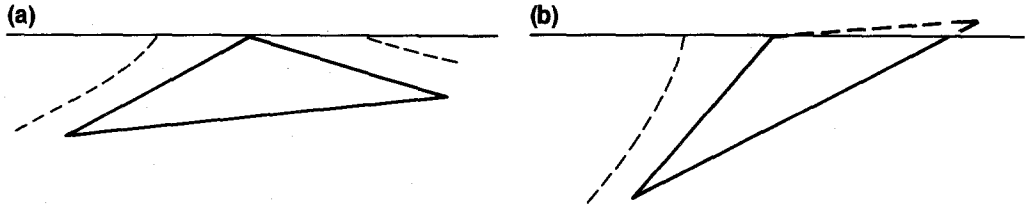

Figure 4 Comparison of partial cone crack profiles from present model (solid lines) with more detailed, step-by-step computations from earlier fracture mechanics analysis (dashed curves). Profiles are for (a) $f = 0.1$, (b) $f = 0.5$, and $\alpha = 22°$.

our final strength formulation shall prove to be insensitive to variations in friction-related quantities.

2.2. Strength

With the above methodology for predetermining crack sizes and shapes in sliding contact events we may proceed directly to an analysis of strength degradation [4]. The basis equation for the strength of a specimen containing a a contact-induced flaw of dimension, c', and inclination, α', is

$$\sigma = K_c/\psi c'^{1/2} \quad (4)$$

where $\psi = \psi(\alpha')$ is a dimensionless geometrical parameter. It is assumed in this formulation that fracture occurs under equilibrium conditions ("inert" strength). It is also assumed that the partial cones are oriented for maximum tension at the deepest point on their bases, i.e. the tensile axis is coincident with the sliding direction, once more consistent with "worst-case" requirements. Then Equations 3 and 4 may be combined to obtain a strength equation of the form

$$\sigma = K_c^{4/3} F(f)_\alpha / P^{1/3} \quad (5)$$

where F is a dimensionless function of f for a given value of α. The dependence on K_c and P in this equation is identical to that for purely normal loading.

This leaves us only with the frictional function $F(f)_\alpha$ to evaluate. The basis for such an evaluation has been laid down elsewhere [1]. Basically, one regards failure as a critical re-initiation process, seeking the incremental configuration at the base of the tilted cone which maximizes the mechanical energy release. In terms of this earlier evaluation we may write $\psi = \lambda\omega^{1/2}$, where λ embodies shape factors (including the effects of the cone crack curvature, interactions with the free surface, etc.) and $\omega = \omega(\alpha') = \omega(f)_\alpha$ defines the rotational component associated with the friction forces. Details of the computation of the ω term are included in the Appendix. The requisite function, which may now be written

$$F(f)_\alpha = 1/\eta^{1/3}\lambda[(1+f^2)^{1/3}\omega(f)_\alpha]^{1/2} \quad (6)$$

is plotted in Fig. 5 for various α. It is immediately clear from Fig. 5 that the strength in Equation 5 is a slowly varying function of friction coefficient, amounting to a factor of only two or three at extremes of the plotting range. Thus for practical purposes it should suffice to determine $F(f)_\alpha$ by graphical interpolation for any prospective sliding contact configuration.

3. Experimental details

In this section we explore the predictions of the above model by running sliding friction tests on soda-lime glass bars. Our choice of glass here simply reflects the convenience of working with a material which is transparent, isotropic and

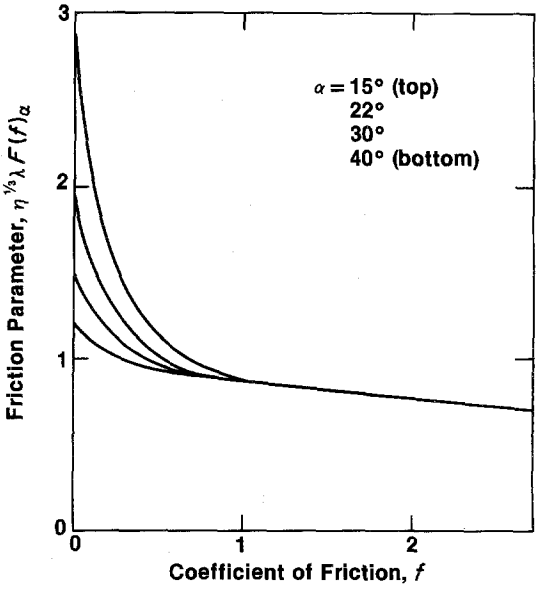

Figure 5 Plot of (normalized) function $F(f)$ in Equation 6 for selected values of α.

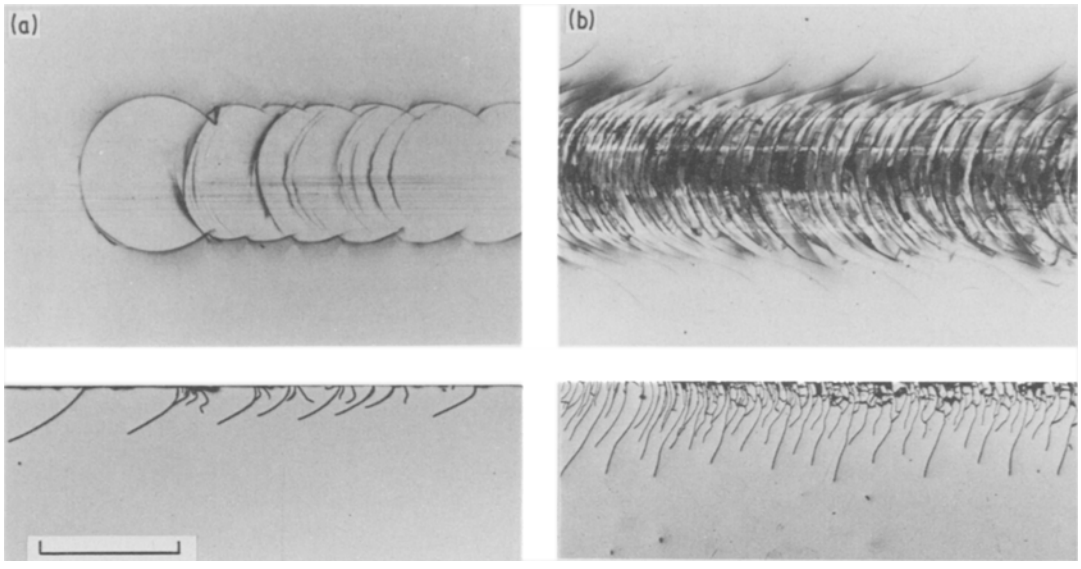

Figure 6 Micrographs showing surface (top) and side (bottom) views of sliding damage on soda-lime glass caused by steel sphere of radius 3.17 mm under normal load $P = 20$ N, for (a) $f = 0.1$, (b) $f = 0.5$. Cf. traces of deep cracks in side views with corresponding theoretical predictions in Fig. 4. Index marker 0.5 mm.

homogeneous. We begin by examining the geometrical features of the damage patterns, and then determine the strength degradation characteristics.

3.1. Geometry of partial cones

Glass bars of surface dimensions 120 by 15 mm were cut from plate of thickness 5.65 mm. Sliding tests were conducted in a simple loading fixture [22] using a steel indenting sphere of radius 3.17 mm. The sphere, rigidly mounted into the end of a vertical arm, was first loaded normally onto the glass surface. Effective lateral translation across the surface was then obtained by activating a horizontal-drive carriage holding the specimen. In our experiments the sliding velocity was fixed at 0.13 mm sec^{-1}, and the translation distance was typically 1 to 3 mm. The specimen was mounted such that the track produced was located at a face centre and oriented parallel to the long edges of the bar. Both normal and tangential loads were monitored continuously using conventional strain gauge cells, thus allowing the friction coefficient to be specified at any point along the track. The range of normal loads covered was 50 to 300 N. Most of the tests were carried out in air, but some were run with liquid lubricants on the glass surface (e.g. water, acetone, silicone oil) [16] to provide a broader spectrum of friction conditions.

The pertinent features of the sliding contact patterns are evident in the micrographs shown in Figs. 6 and 7. Fig. 6 illustrates the more general of these features, for two values of f. The surface views typify the well-documented distortions from

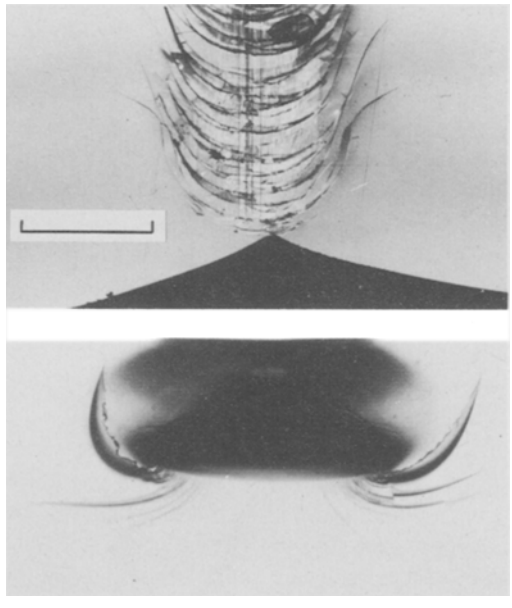

Figure 7 Micrographs showing surface (top) and end (bottom) views of sliding track on glass after strength testing. In this example failure initiated from the first partial cone along track. Track produced by steel sphere under normal load $P = 20$ N, friction coefficient $f = 0.5$. Index marker 0.5 mm.

circular symmetry of the ring crack traces with increasing friction [10]. The side views demonstrate the associated steepening of the trailing cone crack surfaces, in accordance with the frictional dependence of α' in Equation 3b; this observed trend may be correlated visually with the corresponding model representations in Fig. 4. The lengths of the largest subsurface cracks in Fig. 6 are not substantially different for the two cases in Fig. 4, consistent with the insensitivity of c' to f in Equation 3a.

Also evident in Fig. 6 are relatively fine scratch lines which extend along the lengths of the surface tracks. The density of these lines correlates with the friction level. This type of damage is caused by asperities on the sliding sphere. Each such asperity, of course, supports only a minute fraction of the macroscopic normal load, and accordingly acts as a sharp indenter on the microscale. At this scale the local deformation tends to have a predominantly "plastic" component [23], thus explaining the relatively smooth appearance of the linear scratches. These scratches may nevertheless play a far from minor role in the general evolution of partial cone cracks, in that the local microplasticity is capable of generating crack nuclei in its wake [24, 25]. Self-generation processes of this kind ensure the existence of suitable starting flaws for the ensuing partial cone initiation, even on specimens with originally pristine surfaces.

Some variants on the somewhat ideal contact fracture geometries shown in Fig. 6 were observed whenever irregularities occurred in the frictional response. Generally, variations in the value of f along a given track were reflected in the crack density. In cases where tangential forces were applied without sliding, only one or two crescents formed on the surface, but these differed little in general appearance from the first trace in the corresponding sequential crack pattern formed in free translation.

Finally, some crack patterns were formed without any tangential force component acting at all, simply to confirm the value of the crack angle α chosen for the "reference state" in our earlier theoretical calculations. Even under pure normal loading the cone cracks did not always exhibit perfect axial symmetry [11], in which case the angle was measured at the steepest point. The value obtained for our soda-lime glass was $\alpha = 22 \pm 1°$, in agreement with Roesler's determination [19].

3.2. Strength measurements

The strengths of the glass bars were measured in a four-point bend fixture, inner span 38 mm and outer span 107 mm, with the damaged surface on the tensile side. The damage tracks were carefully centred within the inner span and aligned parallel to the direction of maximum tension. Dry nitrogen gas was flushed over the tracks prior to applying the bending stress, and the specimens then taken to failure in < 10 sec, to ensure near-equilibrium conditions of fracture [26]. The resulting "inert" strengths were calculated from the bending force and specimen dimensions using standard thin beam formulae.

After breaking, each track was examined to determine the point at which failure initiated. The normal and tangential forces at this point were then evaluated from the load cell records, from which the operative friction coefficient was determined. Although some breaks did initiate from the start of the tracks, about half initiated away from the ends, usually close to regions of friction maxima. In all cases the initiation point could be traced to the base of the critical cone at its deepest point. Thus, in the example of Fig. 7 we can infer the failure origin from the crack morphology: in the end view the tear lines clearly trace back to a central point on the cone periphery; in the top view we see how the crack, after propagating downward and sideways from its origin, has run back to the free surface, intersecting near (but not directly at) the ring crack trace.

The results of the strength measurements are plotted in Fig. 8 as a function of friction coefficient in accordance with Equation 5. In this figure each individual data point at $f > 0$ represents a single test. Different symbols designate the normal loads used, but no distinction is made between the various conditions of tangential loading (e.g. sliding or nonsliding contact, air or liquid environment). The data point with error bar at $f = 0$ represents the mean and standard deviation of 10 specimens indented under purely normal loading at $P = 30$ N. This last point serves as a reference level for normalizing the friction function $F(f)_\alpha$ in Equation 6, accordingly plotted as the solid curve in Fig. 8. The predicted curve appears to represent the data trend within the bounds of experimental variation, erring, if anything, on the side of conservative design.

4. Discussion

We have developed a simple model for predeter-

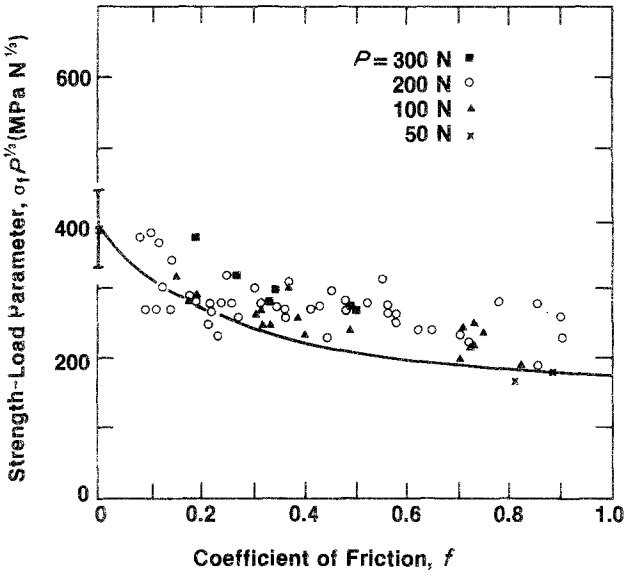

Figure 8 Plot of $\sigma P^{1/3}$ against f for glass subjected to sliding contact with steel sphere at specified loads.

mining the strength degradation characteristics of brittle components subjected to sliding contact damage. We have avoided the usual complexities of a full-scale fracture mechanics analysis by adopting the well-established Roseler solution for pure normal loading as a reference state, and applying a straightforward coordinate transformation to this solution. The transformation is manifested in the formulation for the degraded strength as the multiplicative friction function $F(f)_\alpha$, which may be evaluated directly from plots such as those in Fig. 5. The special appeal of this approach lies in the prospect of characterizing the potential sliding contact response of a given material from normal load data alone, in much the same way as in the generation of the theoretical curve in Fig. 8. Accordingly, the need for access to extensive frictional testing facilities in materials evaluation programs is greatly lessened.

The main conclusion to be drawn from the present study is that frictional effects play a relatively minor role in strength degradation once the threshold for cone cracking is exceeded. The threshold condition itself is, of course, much more sensitive to the level of friction [10, 17]. It could be argued that reduction in friction forces should be a prime design goal, to avoid initiation in the first place. However, this approach could be counter-productive. Raising the critical loading for initiation simultaneously increases the energy available for any ensuing propagation; hence a single, unusually severe contact event could produce an even more dramatic loss of strength than before. In this context we may recall that some contacts are capable of generating their own starting flaws, especially at sharp points or edges on the indenter (Section 3.1).

Consequently, the most conservative designer would assume that initiation is inevitable, in which case the influence of frictional effects in strength amounts to no more than a factor of two or three. This factor may be somewhat reduced by crack–crack interaction effects where the density of damage along the track is high, possibly accounting for the tendency of data points at high f to lie above the theoretical curve in Fig. 8. However, the fact that end failures were not dominant in our sliding experiments would appear to provide adequate justification for ignoring such effects in the strength formulation.

The theoretical model also makes explicit predictions concerning material properties. Clearly, there is considerable advantage to be gained by selecting materials with high toughness, K_c. Poisson's ratio is a parameter with minor influence, via the cone inclination angle term, α. These material aspects of the sliding contact problem will be taken up in greater depth elsewhere [22].

Our model has considered only blunt indenters, but the above conclusions concerning friction and material properties in the strength characterization are expected to have a certain generality. Once the contact-induced cracks penetrate into the far field the distinction between "blunt" and "sharp" becomes somewhat blurred; the stresses remote from the contact are relatively insensitive to con-

ditions at the contact [18]. The main differences are likely to arise in crack geometry terms, hence in the frictional function $F(f)$ in Equation 5, although the presence of residual contact stresses is an added complication with sharp indenters [27, 28].

Acknowledgements

The authors wish to thank J. S. Nadeau for discussions on aspects of this work. Funding for this work was provided by the US Office of Naval Research, Metallurgy and Ceramics Program.

Appendix

Here we reproduce a calculation from the Appendix of [1], with slightly modified notation. Our specific aim is to determine the failure conditions for the partial cone configuration in Fig. 3. Thus the pertinent variables are the cone dimension, c', and inclination, α', and the uniform applied tensile stress, σ_a, which leads to critical extension. It is assumed that the tensile direction is collinear with the length of the sliding track, so that initiation occurs from the deepest point on the cone base.

Our approach is to treat the critical extension as a re-initiation process in the field of the starting cone crack [29]. The stress intensity factors for an inclined crack in uniform tension are [30]

$$\begin{aligned} K_I &= \lambda\sigma_a c'^{1/2} \sin^2 \alpha' \\ K_{II} &= \lambda\sigma_a c'^{1/2} \sin \alpha' \cos \alpha' \end{aligned} \quad \text{(A1)}$$

where λ is a dimensionless shape factor. In general, the crack will not extend in its own plane, but at some tilt angle θ. The local stresses on any such elemental crack increment has both opening (mode I) and sliding (mode II) components [29]

$$\begin{aligned} \sigma_{\theta\theta} &= [K_I/(2\pi r)^{1/2}] f^I_{\theta\theta} + [K_{II}/(2\pi r)^{1/2}] f^{II}_{\theta\theta} \\ &= K'_I/(2\pi r)^{1/2} \\ \sigma_{r\theta} &= [K_I/(2\pi r)^{1/2}] f^I_{r\theta} + [K_{II}/(2\pi r)^{1/2}] f^{II}_{r\theta} \\ &= K'_{II}/(2\pi r)^{1/2} \end{aligned} \quad \text{(A2)}$$

where r is the radial distance from the cone crack tip. The f terms are the angular components of the standard crack-tip stress formulae [29, 30]

$$\begin{aligned} f^I_{\theta\theta} &= \cos^3 (\theta/2) \\ f^I_{r\theta} &= \sin (\theta/2) \cos^2 (\theta/2) \end{aligned} \quad \text{(mode I)} \quad \text{(A3)}$$

$$\begin{aligned} f^{II}_{\theta\theta} &= -3 \sin (\theta/2) \cos^2 (\theta/2) \\ f^{II}_{r\theta} &= \cos (\theta/2)[1 - 3 \sin^2 (\theta/2)] \end{aligned} \quad \text{(mode II)} \quad \text{(A4)}$$

and the "transformed stress intensity factors" K'_I and K'_{II} define the field for the modified crack. Combining Equations A1 and A2 gives

$$\begin{aligned} K'_I &= \lambda\sigma_a c'^{1/2} [f^I_{\theta\theta} \sin^2 \alpha' + f^{II}_{\theta\theta} \sin \alpha' \cos \alpha'] \\ K'_{II} &= \lambda\sigma_a c'^{1/2} [f^I_{r\theta} \sin^2 \alpha' + f^{II}_{r\theta} \sin \alpha' \cos \alpha'] \end{aligned} \quad \text{(A5)}$$

The value of θ appropriate to a given cone inclination α' is determined as that for which the mechanical energy release rate

$$G(\theta, \alpha') = [(1 - \nu^2)/E](K'^2_I + K'^2_{II}) \quad \text{(A6)}$$

is a maximum, ν being Poisson's ratio and E Young's modulus. The requirement $\partial G/\partial\theta = 0$ in Equations A3 to A6 gives the critical value of G,

$$G_c = [(1 - \nu^2)\lambda^2\sigma^2 c'/E]\omega(\alpha') \quad \text{(A7)}$$

where $\sigma = \sigma_a$ is the corresponding critical applied stress, i.e. the "strength", and $\omega(\alpha')$ is a dimensionless function of α' (value unity for normal cracks, i.e. $\alpha' = \pi/2$).

For crack extension under equilibrium conditions, we have [29]

$$G_c = (1 - \nu^2)K_c^2/E \quad \text{(A8)}$$

with K_c the toughness. Comparison of Equations A7 and A8 then leads us to the strength formula, Equation 4, in the text, with

$$\psi = \lambda\omega^{1/2} \quad \text{(A9)}$$

Frictional variations are therefore manifested exclusively via the ω term (the "shape" of the crack, hence λ, being assumed invariant), in accordance with Equation 3, i.e. $\omega = \omega(\alpha') = \omega(f)_\alpha$. This term is most readily determined from the above formulation by numerical analysis [1].

References

1. B. R. LAWN, S. M. WIEDERHORN and H. H. JOHNSON, *J. Amer. Ceram. Soc.* 58 (1975) 428.
2. B. R. LAWN, E. R. FULLER and S. M. WIEDERHORN, *ibid.* 59 (1976) 193.
3. S. M. WIEDERHORN and B. R. LAWN, *ibid.* 60 (1977) 451.
4. B. R. LAWN and D. B. MARSHALL, in "Fracture Mechanics of Ceramics", Vol. 3, edited by R. C. Bradt, D. P. H. Hasselman and F. F. Lange (Plenum Press, New York, 1978) p. 205.
5. S. M. WIEDERHORN and B. R. LAWN, *J. Amer. Ceram. Soc.* 62 (1979) 66.
6. D. W. RICHERSON and K. M. JOHANSEN, "Ceramic Gas Turbine Engine Demonstration Program", Final Report to Department of the Navy (U.S.), Garrett Corporation, Report No. 21-4410 (1982).

7. D. W. RICHERSON, W. D. CARRUTHERS and L. J. LINDBERG, in "Surfaces and Interfaces in Ceramic and Ceramic–Metal Systems", edited by J. A. Pask and A. G. Evans (Plenum Press, New York, 1980) p. 661.
8. D. W. RICHERSON, D. G. FINGER and J. M. WIMMER, in "Fracture Mechanics of Ceramics", Vol. 5, edited by R. C. Bradt, A. G. Evans, D. P. H. Hasselman and F. F. Lange (Plenum Press, New York, 1983).
9. G. M. HAMILTON and L. E. GOODMAN, *J. Appl. Mech.* **33** (1966) 371.
10. B. R. LAWN, *Proc. Roy. Soc. Lond.* **A299** (1967) 307.
11. F. C. FRANK and B. R. LAWN, *ibid.* **A299** (1967) 291.
12. D. R. GILROY and W. HIRST, *J. Phys. D: Appl. Phys.* **2** (1969) 1784.
13. B. D. POWELL and D. TABOR, *ibid.* **3** (1970) 783.
14. W. E. SWINDLEHURST and T. R. WILSHAW, *J. Mater. Sci.* **11** (1976) 1183.
15. B. BETHUNE, *ibid.* **11** (1976) 199.
16. Y. ENOMOTO, *ibid.* **16** (1981) 3365.
17. S. CHIANG and A. G. EVANS, *J. Amer. Ceram. Soc.* **66** (1983) 4.
18. B. R. LAWN and T. R. WILSHAW, *J. Mater. Sci.* **10** (1975) 1049.
19. F. C. ROESLER, *Proc. Phys. Soc. Lond.* **B69** (1956) 55.
20. B. R. LAWN and E. R. FULLER, *J. Mater. Sci.* **10** (1975) 2016.
21. B. R. LAWN and H. KOMATSU, *Phil. Mag.* **14** (1966) 689.
22. S. M. WIEDERHORN, B. R. LAWN, J. S. NADEAU and D. E. ROBERTS to be published.
23. B. R. LAWN and D. B. MARSHALL, *J. Amer. Ceram. Soc.* **62** (1979) 347.
24. B. R. LAWN and A. G. EVANS, *J. Mater. Sci.* **12** (1977) 2195.
25. B. R. LAWN, T. P. DABBS and C. J. FAIRBANKS, *ibid.* in press.
26. T. P. DABBS, B. R. LAWN and P. L. KELLY, *Phys. Chem. Glasses* **23** (1982) 58.
27. D. B. MARSHALL and B. R. LAWN, *J. Mater. Sci.* **14** (1979) 2001.
28. D. B. MARSHALL, B. R. LAWN and P. CHANTIKUL, *ibid.* **14** (1979) 2225.
29. B. R. LAWN and T. R. WILSHAW, "Fracture of Brittle Solids" (Cambridge University Press, London, 1975) Chap. 3.
30. P. C. PARIS and G. C. SIH, in "Fracture Toughness Testing and its Applications", ASTM STP 381 (American Society for Testing and Materials, Philadelphia, 1964) p. 30.

Received 10 October
and accepted 26 October 1983